# Improvements and limitations of Mie n-6 force fields for predicting liquid shear viscosity at saturation and elevated pressures

Richard A. Messerly

*Thermodynamics Research Center, National Institute of Standards and Technology, Boulder, Colorado, 80305*

Michelle C. Anderson

*Thermodynamics Research Center, National Institute of Standards and Technology, Boulder, Colorado, 80305*

S. Mostafa Razavi

*Department of Chemical and Biomolecular Engineering, The University of Akron*

J. Richard Elliott

*Department of Chemical and Biomolecular Engineering, The University of Akron*

## Abstract

To determining reliable methodologies and models for the estimation of viscosities, equilibrium molecular dynamics simulations for normal and branched alkanes ranging from two to sixteen carbons were performed with the GROMACS package. Viscosities along the liquid/vapor saturation curve and at 293 K and high-pressure conditions were generated using the TraPPE, Potoff, and TAMie force fields. Viscosities were calculated from simulations using the Green-Kubo method. Reliable data and uncertainties were determined by performing many replicate simulations and analyzing the data distributions. Potoff and TAMie, modern force fields making use of the Mie n-6 (the generalized Lennard-Jones 12-6 potential), outperform the older TraPPE force field which makes use of the traditional Lennard-Jones 12-6 potential. Simulations carried out with the Potoff or TAMie potentials more closely follow trends in viscosity. The TraPPE force field consistently under predicts viscosities. Although

*Email addresses:* richard.messerly@nist.gov (Richard A. Messerly), michelle.anderson@nist.gov (Michelle C. Anderson), sr87@uakron.edu (S. Mostafa Razavi), elliot1@uakron.edu (J. Richard Elliott)

simulations with the Potoff force field overestimate viscosity with respect to density, a for-
tuitous cancellation of errors results in good prediction of viscosity with respect to pressure.
The performance of the TAMie force field is usually better than TraPPE but slightly worse
than Potoff. All force fields perform somewhat better for normal alkanes than for branched
alkanes and the differences in performance between force fields is more noticeable in the case
of normal alkanes.

## 1. Introduction

The design of efficient and reliable technical processes requires accurate estimates of
thermophysical properties. Shear viscosity ($\eta$) is an important property for characterizing
flow, e.g. sizing pumps. There are primarily three different means by which shear viscosity
estimates are obtained: experimental measurement, semi-empirical model prediction, and
molecular simulation (molecular dynamics, MD). Significant limitations exist for each of these
methods. For example, experimental measurements can be expensive, time-consuming, and
challenging at extreme temperatures ($T$) and pressures ($P$). Semi-empirical models often
struggle from poor extrapolation due to model deficiencies, over-fitting, and the scarcity
of *reliable* experimental data over a wide range of $P\rho T$ state space. Molecular dynamics
requires extremely reliable force fields and robust simulation methods.

There are two fundamental challenges for utilizing molecular simulation to estimate vis-
cosity. First, obtaining reproducible results is more difficult for transport properties, such as
viscosity, than for static properties. Second, viscosity is extremely sensitive to the force field.
In addition to the strong dependence on the intermolecular interactions, the intramolecular
potential plays a much greater role for viscosity than for static properties. For example,
varying the torsional potential has a significant impact on viscosity while vapor-liquid coex-
istence is relatively unaffected. Therefore, the ability to predict viscosities with molecular
simulation requires both robust methods and adequate force fields.

Recently, a "Best Practices Guide" was developed to address the first challenge, namely,

to improve reproducibility. While we apply the "Best Practices", the focus of this study is the second challenge. Specifically, we investigate the accuracy of united-atom Mie n-6 force fields, a popular class designed for the engineering purpose of predicting thermophysical properties. The suitability of these force fields for quantitative viscosity prediction has been widely debated in the literature. For example, BLANK suggested that united-atom models are inadequate for this purpose and recommended the use of all-atom models. By contrast, BLANK suggested that great improvement is obtained by utilizing a Mie n-6 potential over the traditional Lennard-Jones 12-6 potential. However, these studies focused on viscosities of saturated liquids. Recently, it was shown that Mie n-6 potentials are overly repulsive at high densities/pressures. For these reasons, we study how well the united-atom Mie n-6 potentials perform both at saturation and elevated pressures.

Furthermore, BLANK demonstrated that it is important to include viscosity data when parameterizing a Mie n-6 force field to obtain a unique set of transferable parameters. The force fields compared in this study were optimized solely with static vapor-liquid coexistence data, e.g., saturated liquid densities and saturated vapor pressures. Therefore, an additional purpose of this study is to determine the transferability of these force fields that were not parameterized without viscosity data.

The outline for the present work is the following. Section 2 explains the force fields, simulation methodology, and data analysis. Section 3 presents the simulation results for each force field, compound, and state point studied. Section 4 discusses some important observations and limitations. Section 5 recaps the primary conclusions from this work.

## 2. Methods

### 2.1. Force field

A united-atom (UA) or anisotropic-united-atom (AUA) representation is used for each compound studied. UA models assume that the UA interaction site is that of the carbon atom, while AUA models assume that the AUA interaction site is shifted away from the carbon atom and towards the hydrogen atom(s). Note that TraPPE and Potoff are UA force fields while TraPPE-2, AUA4, and TAMie are AUA force fields.

The UA and AUA groups required for normal and branched alkanes are sp$^3$ hybridized CH$_3$, CH$_2$, CH, and C sites. For most literature models, a single (transferable) parameter set is assigned for each interaction site. However, two exceptions exist for the force fields studied. First, TAMie implements a different set of CH$_3$ parameters for ethane. Second, Potoff reports a "generalized" and "short/long" (S/L) CH and C parameter set. The Potoff "generalized" CH and C parameter set is an attempt at a completely transferable set. However, since the "generalized" parameters performed poorly for some compounds, the S/L parameter set was proposed, where the "short" and "long" parameters are implemented when the number of carbons in the backbone is $\leq 4$ and $> 4$, respectively.

A fixed bond-length is used for each bond between UA or AUA sites. Note that, although static thermodynamic properties are generally insensitive to the choice of fixed or flexible bonds, dynamic properties, such as viscosity, are much more sensitive. For this reason, we test the degree of variability that arises by implementing a harmonic oscillator model. The results are provided as Supporting Information.

Although TAMie is an AUA force field, only the terminal CH$_3$ sites have a displacement in the interaction site. This convention is much simpler to implement than other AUA approaches (such as AUA4) where non-terminal (i.e. CH$_2$ and CH) interaction sites also have a displacement distance. For this reason, we do not attempt to simulate the AUA4 force field for any compounds containing CH$_2$ and CH interaction sites. For the compounds and force fields simulated, the anisotropic shift in a terminal interaction site (i.e. CH$_3$) is treated simply as a longer effective bond-length (see Table 1). The bond-length for all non-terminal sites is 0.154 nm.

The angle and dihedral energies are computed using the same functional forms for each force field. Angular bending interactions are evaluated using a harmonic potential:

$$u^{\text{bend}} = \frac{k_\theta}{2} \left(\theta - \theta_0\right)^2 \tag{1}$$

where $u^{\text{bend}}$ is the bending energy, $\theta$ is the instantaneous bond angle, $\theta_0$ is the equilibrium bond angle, and $k_\theta$ is the harmonic force constant which is equal to 62500 K/rad$^2$ for all

Table 1: Effective bond-lengths in units of nm for terminal (CH$_3$) UA or AUA interaction sites. Empty table entries for TraPPE-2 denote that the force field does not contain the corresponding interaction site type. Empty table entries in AUA4 arise because this force field uses a more complicated construction than the simple effective bond-length approach. Specifically, AUA4 requires CH$_2$ and CH interaction sites that are not along the C-C bond axis.

| Bond | TraPPE, Potoff | TAMie | AUA4 | TraPPE-2 |
|---|---|---|---|---|
| CH$_3$-CH$_3$ | 0.154 | 0.194 | 0.1967 | 0.230 |
| CH$_3$-CH$_2$ | 0.154 | 0.174 | – | – |
| CH$_3$-CH | 0.154 | 0.174 | – | – |
| CH$_3$-C | 0.154 | 0.174 | 0.1751 | – |

bonding angles. Dihedral torsional interactions are determined using a cosine series:

$$u^{\text{tors}} = c_0 + c_1[1 + \cos \phi] + c_2[1 - \cos 2\phi] + c_3[1 + \cos 3\phi] \tag{2}$$

where $u^{\text{tors}}$ is the torsional energy, $\phi$ is the dihedral angle and $c_i$ are the Fourier constants. The equilibrium bond angles and torsional parameters are found in Tables 2-3, respectively.

Table 2: Equilibrium bond angles ($\theta_0$). $x$ and $y$ are values between 0-3.

| Bending sites | $\theta_0$ (degrees) |
|---|---|
| CH$_x$-CH$_2$-CH$_y$ | 114.0 |
| CH$_x$-CH-CH$_y$ | 112.0 |
| CH$_x$-C-CH$_y$ | 109.5 |

Non-bonded interaction energies and forces between sites located in two different molecules or separated by more than three bonds are calculated using a Mie n-6 potential (of which the Lennard-Jones, LJ, 12-6 is a subclass) [1]:

$$u^{\text{vdw}}(\epsilon, \sigma, n; r) = \left(\frac{n}{n-6}\right) \left(\frac{n}{6}\right)^{\frac{6}{n-6}} \epsilon \left[\left(\frac{\sigma}{r}\right)^n - \left(\frac{\sigma}{r}\right)^6\right] \tag{3}$$

Table 3: Fourier constants ($c_i$) in units of K. $x$ and $y$ are values between 0-3.

| Torsion sites | $c_0$ | $c_1$ | $c_2$ | $c_3$ |
|---|---|---|---|---|
| $CH_x$-$CH_2$-$CH_2$-$CH_y$ | 0.0 | 355.03 | -68.19 | 791.32 |
| $CH_x$-$CH_2$-CH-$CH_y$ | -251.06 | 428.73 | -111.85 | 441.27 |
| $CH_x$-$CH_2$-C-$CH_y$ | 0.0 | 0.0 | 0.0 | 461.29 |
| $CH_x$-CH-CH-$CH_y$ | -251.06 | 428.73 | -111.85 | 441.27 |

where $u^{\text{vdw}}$ is the van der Waals interaction, $\sigma$ is the distance ($r$) where $u^{\text{vdw}} = 0$, $-\epsilon$ is the energy of the potential at the minimum $\left(\text{i.e. } u^{\text{vdw}} = -\epsilon \text{ and } \frac{\partial u^{\text{vdw}}}{\partial r} = 0 \text{ for } r = r_{\min}\right)$, and n is the repulsive exponent. The non-bonded Mie n-6 force field parameters for TraPPE, TraPPE-2, Potoff, AUA4, and TAMie are provided in Table 4.

Table 4: Non-bonded (intermolecular) parameters for TraPPE [2, 3] (and TraPPE-2 [4]), Potoff [5, 6], AUA4 [7, 8], and TAMie [9, 10] force fields. The "short/long" Potoff CH and C parameters are included in parentheses. The ethane specific parameters for TAMie are included in parentheses.

| United-atom | TraPPE (TraPPE-2) | | | Potoff (S/L) | | |
|---|---|---|---|---|---|---|
| | $\epsilon$ (K) | $\sigma$ (nm) | n | $\epsilon$ (K) | $\sigma$ (nm) | n |
| $CH_3$ | 98 (134.5) | 0.375 (0.352) | 12 | 121.25 | 0.3783 | 16 |
| $CH_2$ | 46 | 0.395 | 12 | 61 | 0.399 | 16 |
| CH | 10 | 0.468 | 12 | 15 (15/14) | 0.46 (0.47/0.47) | 16 |
| C | 0.5 | 0.640 | 12 | 1.2 (1.45/1.2) | 0.61 (0.61/0.62) | 16 |
| | AUA4 | | | TAMie | | |
| $CH_3$ | 120.15 | 0.3607 | 12 | 136.318 (130.780) | 0.36034 (0.36463) | 14 |
| $CH_2$ | 86.29 | 0.3461 | 12 | 52.9133 | 0.40400 | 14 |
| CH | 50.98 | 0.3363 | 12 | 14.5392 | 0.43656 | 14 |
| C | 15.04 | 0.244 | 12 | – | – | – |

Non-bonded interactions between two different site types (i.e. cross-interactions) are determined using Lorentz-Berthelot combining rules [11] for $\epsilon$ and $\sigma$, respectively, and an arithmetic mean for the repulsive exponent n (as recommended in Reference 5):

$$\epsilon_{ij} = \sqrt{\epsilon_{ii}\epsilon_{jj}} \tag{4}$$

$$\sigma_{ij} = \frac{\sigma_{ii} + \sigma_{jj}}{2} \tag{5}$$

$$n_{ij} = \frac{n_{ii} + n_{jj}}{2} \tag{6}$$

where the $ij$ subscript refers to cross-interactions and the subscripts $ii$ and $jj$ refer to same-site interactions.

### 2.2. Simulation set-up

Viscosity estimates can be obtained from both equilibrium molecular dynamics (EMD) and non-equilibrium molecular dynamics (NEMD) simulations. The "Best Practices Guide" is currently limited to EMD methods and purports that NEMD might be necessary for high viscosities (greater than 0.02 Pa-s). One purpose of the present work is to demonstrate that, by applying these guidelines, EMD can also provide meaningful estimates for highly viscous systems.

Equilibrium molecular dynamics simulations are performed using GROMACS version 2018 [12]. Example GROMACS input files (.top, .gro. and .mdp) are provided as Supporting Information. In addition, the shell and python scripts used for preparing and analyzing simulations are available on GitHub. The simulation specifications are provided in Tables 5 and 6.

Note that the non-bonded cut-off distance is 1.4 nm for each force field except Potoff, which employs a 1.0 nm cut-off (as recommended by the authors). Also, notice that the production time depends on the system, i.e., the compound and state point, where larger compounds, lower temperatures, and higher densities necessitate longer simulations. For most systems, 1 ns is a sufficient production time, while an 8 ns production time is required for the most viscous systems, e.g., 2,2,4-trimethylpentane at elevated pressures. Following

7

Table 5: General simulation specifications.

| | |
|---|---|
| Time-step (fs) | 2 |
| Equilibration time (ns) | 1 |
| Production time (ns) | 1, 2, 4, or 8 |
| Cut-off length (nm) | 1.4 (1.0 Potoff) |
| Tail-corrections [13] | $U$ and $P$ |
| Constraints | LINCS |
| LINCS-order | 8 |
| Number of molecules | 400 |

Table 6: Integrator, thermostat and barostat specifications.

| | $NPT$ Equil. | $NPT$ Prod. | $NVT$ Equil. | $NVT$ Prod. |
|---|---|---|---|---|
| Integrator | Velocity Verlet | Leap frog | Velocity Verlet | Velocity Verlet |
| Thermostat | Velocity rescale | Nosé-Hoover | Nosé-Hoover | Nosé-Hoover |
| Thermostat time-constant (ps) | 1.0 | 1.0 | 1.0 | 1.0 |
| Barostat | Berendsen | Parrinello-Rahman | N/A | N/A |
| Barostat time-constant (ps) | 1.0 | 5.0 | N/A | N/A |
| Barostat compressibility | 4.5e-5 | 4.5e-5 | N/A | N/A |

"Best Practices", we compute $\eta$ with several different production times (1, 2, 4, and 8 ns) for select systems to verify that the results are indistinguishable (see Supporting Information). Furthermore, we investigate system size effects by comparing results with 100, 200, 400, and 800 molecules (see Supporting Information). In addition, we compare fixed and flexible bonds in the Supporting Information.

As recommended by "Best Practices," we utilize 30 to 60 independent replicates to improve the precision and to provide more rigorous estimates of uncertainty. To ensure inde-

pendence between replicates, a series of MD simulations are performed for each replicate. When the viscosity is desired at a prescribed temperature and density ($\eta(\rho, T)$), three stages are required: energy minimization, $NVT$ equilibration, and $NVT$ production. When the viscosity is desired at a prescribed temperature and pressure ($\eta(P, T)$), five stages are required: energy minimization, $NPT$ equilibration, $NPT$ production, $NVT$ equilibration, and $NVT$ production. Note that, according to "Best Practices", the final production stage simulations are always performed using the $NVT$ ensemble.

Two different classes of viscosity are investigated in this study, namely, saturated liquid viscosity ($\eta_{\text{liq}}^{\text{sat}}$) and compressed liquid viscosities at $T = 293$ K ($\eta_{\text{liq}}^{\text{comp}}$).

Saturated liquid viscosities are estimated by performing $NVT$ ensemble simulations at various temperatures ($T^{\text{sat}}$) and densities ($\rho_{\text{liq}}^{\text{sat}}$). The simulation densities correspond to the REFPROP $\rho_{\text{liq}}^{\text{sat}}$, which is admittedly not equivalent to the force field $\rho_{\text{liq}}^{\text{sat}}$. This point is discussed in greater detail in Section 4.

Two different simulation protocols are implemented for estimating compressed liquid viscosities ($\eta_{\text{liq}}^{\text{comp}}$). Specifically, we perform simulations with each force field either at the same $\rho$ or the same $P$. For the purpose of comparing trends between force fields and REFPROP, these two methods are essentially equivalent. From a practical standpoint, estimating $\eta$ at a given $P$ requires performing preliminary $NPT$ ensemble simulations to determine the corresponding box size.

### 2.3. Data analysis

Following the "Best Practices" recommendation, we implement the Green-Kubo "time-decomposition" analysis to extract viscosity from EMD simulations. We refer the interested reader to References BLANK and BLANK for further details. In brief, the Green-Kubo integral is computed with respect to time according to

$$\frac{V}{3k_{\text{B}}TN_{\text{reps}}} \sum_{n=1}^{N_{\text{reps}}} \sum_{\alpha \neq \beta} \int_0^{\infty} dt \, \langle \tau_{\alpha\beta,n}(t)\tau_{\alpha\beta,n}(0) \rangle_{t_0} \tag{7}$$

where $V$ is the volume, $k_{\text{B}}$ is the Boltzmann constant, $\langle \cdots \rangle_{t_0}$ denotes an average over time origins, $\alpha$ and $\beta = x, y$, or $z$ Cartesian coordinates, and $\tau_{\alpha\beta,n}$ is the $\alpha$-$\beta$ off-diagonal stress

9

tensor element for the $n^{\text{th}}$ replicate.

$\tau_{\alpha\beta,n}$ is recorded every 6 fs (3 time-steps) to adequately integrate the initial rapid decay of the autocorrelation function. To improve precision, Equation 7 is an average over all three off-diagonal components of the stress tensor, 30 to 60 independent replicate simulations ($N_{\text{reps}}$), and twelve different time-origins ($t_0$) for each replicate.

Since Equation 7 requires $t \to \infty$ and the "running integral" can become quite noisy at long times, it is important to fit the "running integral" to a function that can be extrapolated to the "true" infinite time limit ($\eta^\infty$). Per "Best Practices", we use a double-exponential function for this purpose

$$\eta(t) = A\alpha\tau_1 \left(1 - \exp\left(-t/\tau_1\right)\right) + A(1-\alpha)\tau_2 \left(1 - \exp\left(-t/\tau_2\right)\right) \tag{8}$$

where $A, \alpha, \tau_1$, and $\tau_2$ are fitting parameters and $\eta^\infty = A\alpha\tau_1 + A(1-\alpha)\tau_2$.

To account for the increasing fluctuations in the "running integral" with respect to time, Equation 8 is fit by minimizing a weighted sum-squared error objective function. The weight model, $At^{-b}$, is fit to the standard deviation ($\sigma_\eta$) of the replicate simulations. In addition, following a heuristic proposed by Zhang et al., data are excluded where $\sigma_\eta > 40 \% \, \eta^\infty$. As large fluctuations also exist at very short times, only data for $t > 3$ ps are included in the parameterization of Equation 8.

Uncertainties are obtained by bootstrap re-sampling. Specifically, the process described previously is repeated hundreds of times using randomly selected sets of replicate simulations. Furthermore, each repetition uses a randomly selected long-time cut-off between 30 % $\eta^\infty$ and 50 % $\eta^\infty$. A 95 % confidence interval is obtained from the distribution of bootstrap estimates for $\eta_\infty$. An example of this process is provided as Supporting Information.

## 3. Results

Six normal and seven branched alkanes of varying chain-length and degree of branching are simulated in this study. Specifically, we simulate ethane, propane, $n$-butane, $n$-octane, $n$-dodecane, $n$-hexadecane, 2-methylpropane, 2-methylbutane, 2-methylpentane, 3-methylpentane, 2,2-dimethylpropane, 2,3-dimethylbutane, and 2,2,4-trimethylpentane. These

compounds were chosen to represent a diverse set of normal and branched alkanes which have available REFPROP viscosity correlations [14, 15, 16, 17, 18, 19, 20].

Each compound was simulated using the TraPPE (UA LJ 12-6) and Potoff S/L (UA Mie 16-6) force fields. Potoff "short" parameters are used for 2-methylpropane, 2-methylbutane, 2,2-dimethylpropane, and 2,3-dimethylbutane while Potoff "long" parameters are utilized for 2-methylpentane, 3-methylpentane, and 2,2,4-trimethylpentane. Only 2,2-dimethylpropane was simulated with AUA4 (AUA LJ 12-6) while 2,2-dimethylpropane and 2,2,4-trimethylpentane were not simulated using the TAMie (AUA Mie 14-6) force field.

### 3.1. Saturated Liquid

#### 3.1.1. n-Alkanes

Figure 1 compares the TraPPE (UA LJ 12-6), TraPPE-2 (AUA LJ 12-6), TAMie (AUA Mie 14-6), Potoff (UA Mie 16-6), and the Bayesian parameter sets for $n = 13$, 14, 15, and 16.
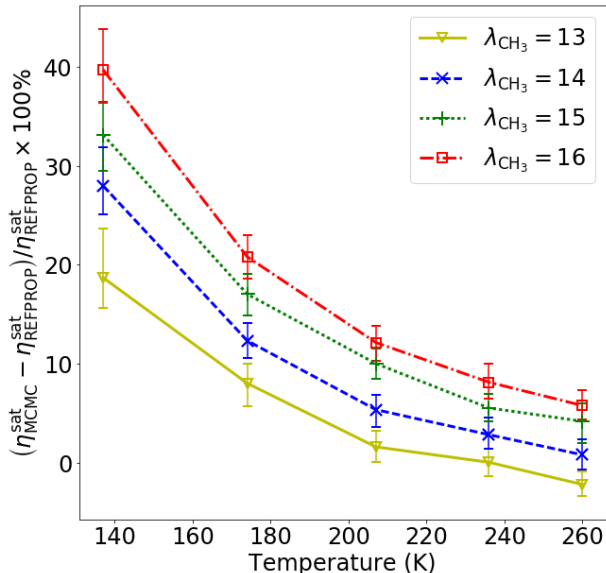


Figure 1: Saturated liquid viscosities for ethane. Colors/symbols denote different force fields.

Figure 2 compares the TraPPE (UA LJ 12-6), Potoff (UA Mie 16-6), and TAMie (AUA Mie 14-6) saturated liquid viscosities for propane, $n$-butane, and $n$-octane. Similar to what

11

has been demonstrated in previous studies, the TraPPE force field significantly under predicts $\eta_{\text{liq}}^{\text{sat}}$ (between 30 and 80 %) with the deviation increasing towards the triple point temperature. By contrast, the Potoff and TAMie force fields agree with the REFPROP values for these compounds to within 10 % over the entire temperature range studied (which includes the triple point for propane), and do not demonstrate a strong temperature dependence.

Figure 3 compares the TraPPE, Potoff, and TAMie saturated liquid viscosities for $n$-dodecane and $n$-hexadecane. Although the TAMie and TraPPE results for these compounds are similar to those observed in Figure 2, it is quite curious that the Potoff results are nearly identical to the TraPPE results for $n$-dodecane (which significantly under predict $\eta^{\text{sat}}$).

### 3.1.2. Branched alkanes

Figures 4 and 5 compare the saturated liquid viscosities for each force field and branched alkane studied. Figures 4 and 5 present results for the compounds classified by Potoff as "short" and "long", respectively. Specifically, Figure 4 depicts 2-methylpropane, 2,2-dimethylpropane, 2-methylbutane, and 2,3-dimethylbutane, while Figure 5 contains 2-methylpentane, 3-methylpentane, and 2,2,4-trimethylpentane. Each compound was simulated using the TraPPE (UA LJ 12-6) and Potoff (UA Mie 16-6) force fields. However, only 2,2-dimethylpropane was simulated with AUA4 (AUA LJ 12-6) while 2,2-dimethylpropane and 2,2,4-trimethylpentane were not simulated using the TAMie (AUA Mie 14-6) force field.

From Figures 4 and 5, we see that the Potoff S/L and TAMie force fields are not as accurate for these branched alkanes as for the normal alkanes. In particular, Potoff and TAMie demonstrates the same temperature dependence observed for other force fields, where the deviations are largest at lower temperatures. However, Potoff still provides considerable improvement compared to the LJ 12-6 based models, i.e., TraPPE and AUA4. Note that the performance is similar for the Potoff "short" and "long" parameters in Figures 4 and 5, respectively.

The deviations for each force field are largest for 2-methylpropane and 2,2-dimethylpropane. Since these compounds are primarily composed of $CH_3$ UA sites, this poor performance is likely due to the assumption that the $CH_3$ non-bonded parameters are transferable from
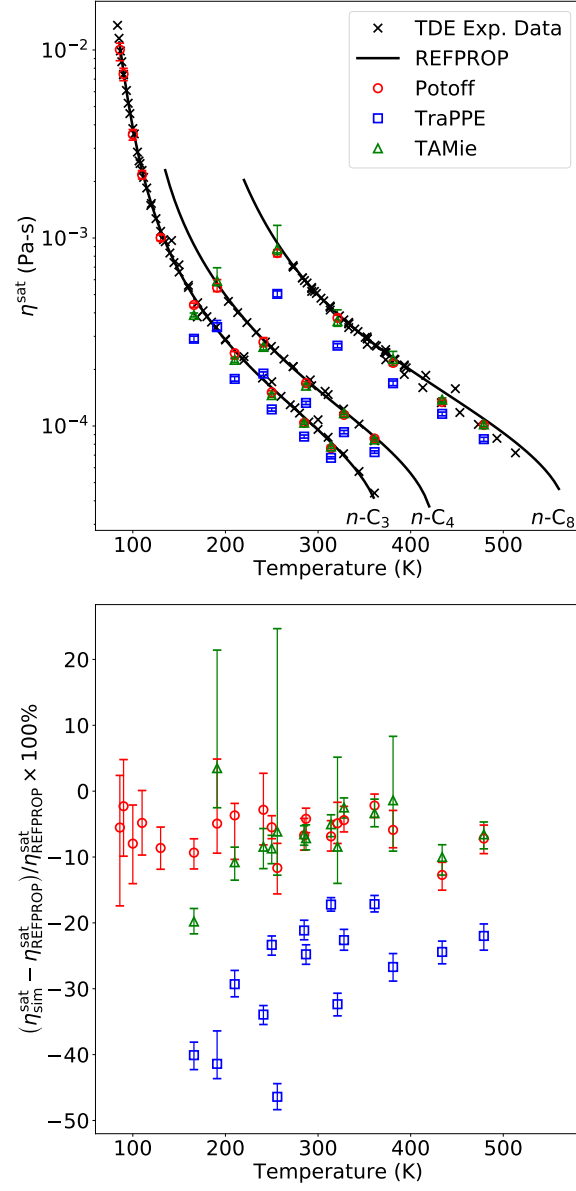
Figure 2: Saturated liquid viscosities for propane, $n$-butane, and $n$-octane. Colors/symbols denote different force fields.

$n$-alkanes to branched alkanes. Improvement might be possible if the $CH_3$ parameters were different depending on the neighboring UA site type.
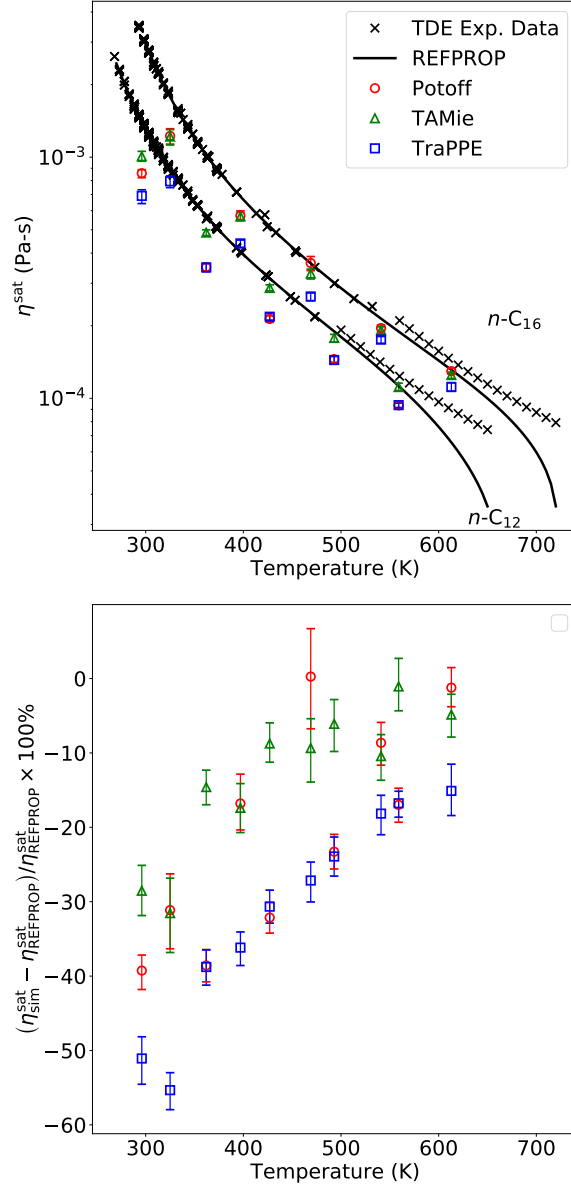
Figure 3: Saturated liquid viscosities for *n*-dodecane and *n*-hexadecane. Colors/symbols denote different force fields.

## 3.2. Compressed liquid

Section 3.1 demonstrated that Mie n-6 based force fields (Potoff and TAMie) are considerably more reliable for predicting saturated liquid viscosities than LJ 12-6 based force fields (TraPPE and AUA4). However, both the Potoff and TAMie non-bonded potentials use
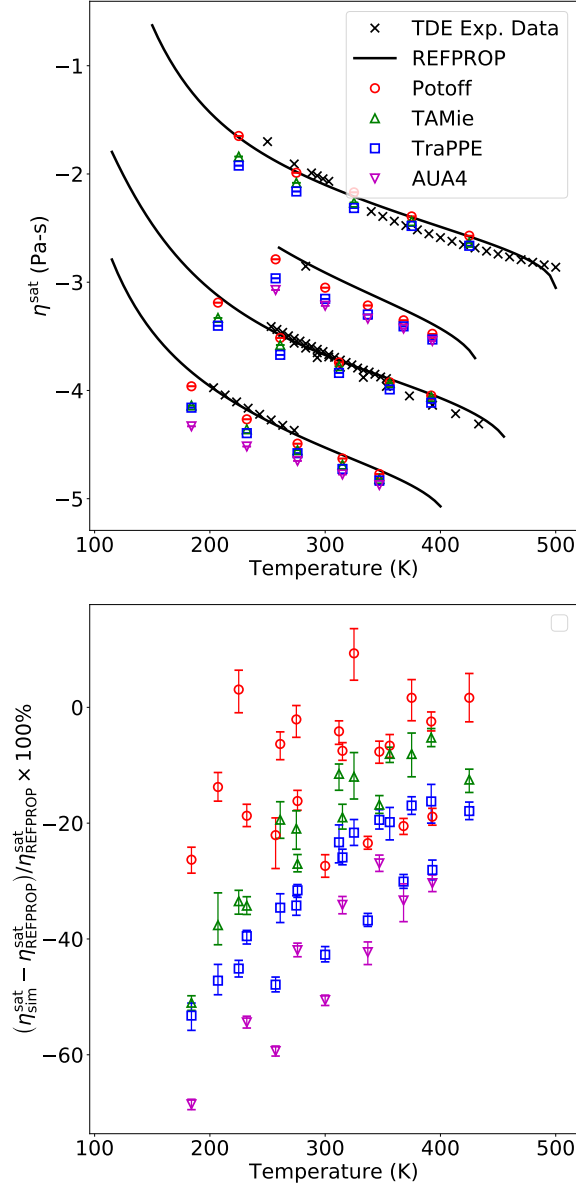
Figure 4: Saturated liquid viscosities for 2-methylpropane, 2,2-dimethylpropane, 2-methylbutane, and 2,3-dimethylbutane. Colors/symbols denote different force fields.

$n > 12$. Reference BLANK demonstrates that $n > 12$ leads to strong negative consequences at high densities/pressures. Specifically, $n > 12$ is too repulsive at short distances which leads to over estimates of pressure at high densities. For this reason, this section compares the different force fields above saturation pressure.

15
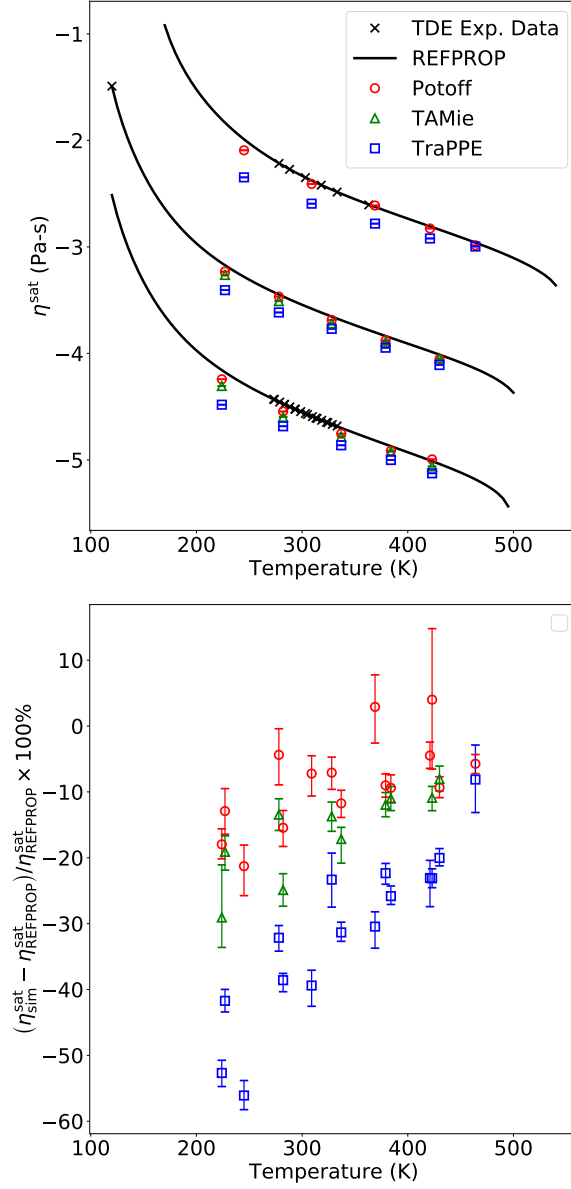
Figure 5: Saturated liquid viscosities for 2-methylpentane, 3-methylpentane, and 2,2,4-trimethylpentane. Colors/symbols denote different force fields.

### 3.2.1. n-Alkanes

Figures 6, 7, and 8 compare the elevated pressure viscosities for propane, $n$-butane, and $n$-octane, respectively. Each compound is simulated using the TraPPE, Potoff, and TAMie force fields. Note that for propane and $n$-butane (Figures 6 and 7) each force field is simulated

at the same density, while for $n$-octane (Figure 8) the force fields are simulated at the same pressure.

Figure 6 demonstrates that the TraPPE force field has a constant negative bias even with increasing density/pressure. The TAMie force field has the most accurate $\eta$-$\rho$ dependence, i.e., the error does not increase with respect to density. By contrast, the Potoff potential demonstrates considerable over estimation of $\eta$ at high densities, which is likely attributed to the overly repulsive Mie 16-6 potential at close distances. Remarkably, the Potoff force field is the most accurate at predicting the $\eta$-$P$ dependence. This can be explained as a cancellation of errors since the Potoff force field significantly over predicts both viscosity and pressure at high densities.

The results in Figures 7 and 8 for $n$-butane and $n$-octane, respectively, are similar to those in Figure 6 for propane. Specifically, the TraPPE force field under predicts $\eta$ at all densities/pressures, the TAMie force field provides the most accurate $\eta$-$\rho$ dependence, while the Potoff force field over predicts $\eta$-$\rho$ dependence but accurately predicts the $\eta$-$P$ dependence.

*3.2.2. Branched alkanes*

The trends observed in Figures 9 to 12 are consistent with the compressed liquid trends for $n$-alkanes. Specifically, TraPPE under-predicts the viscosity with respect to both $\rho$ and $P$. Potoff over-predicts $\eta$ with respect to $\rho$ but provides a reasonable estimate for $\eta$ with respect to $P$. However, as observed previously for saturation viscosities, Potoff and TAMie are less accurate for branched alkanes than for $n$-alkanes.

## 4. Discussion/Limitations

1. Discussion

   (a) Mie potentials parameterized with VLE data provide significant improvement over LJ 12-6

   (b) Potoff over-predicts $\eta - \rho$ dependence while TAMie is fairly accurate

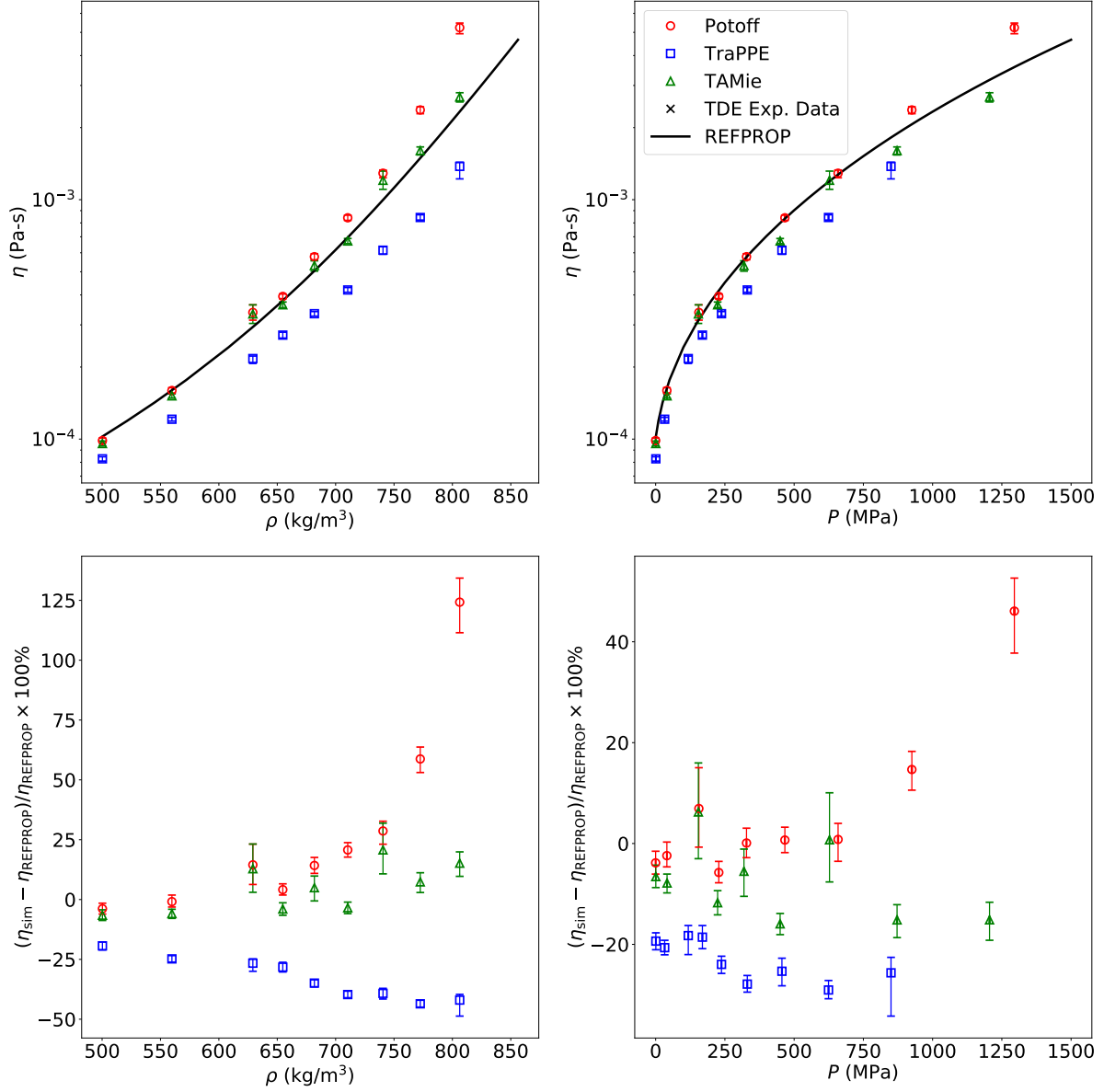   (c) Potoff appears to be slightly more accurate for $\eta - P$

Figure 6: Compressed liquid viscosities at 293 K for propane. Colors/symbols denote different force fields.

    (d) Branched alkanes are not as accurate, perhaps assumption of transferability or torsional parameters

2. Limitations

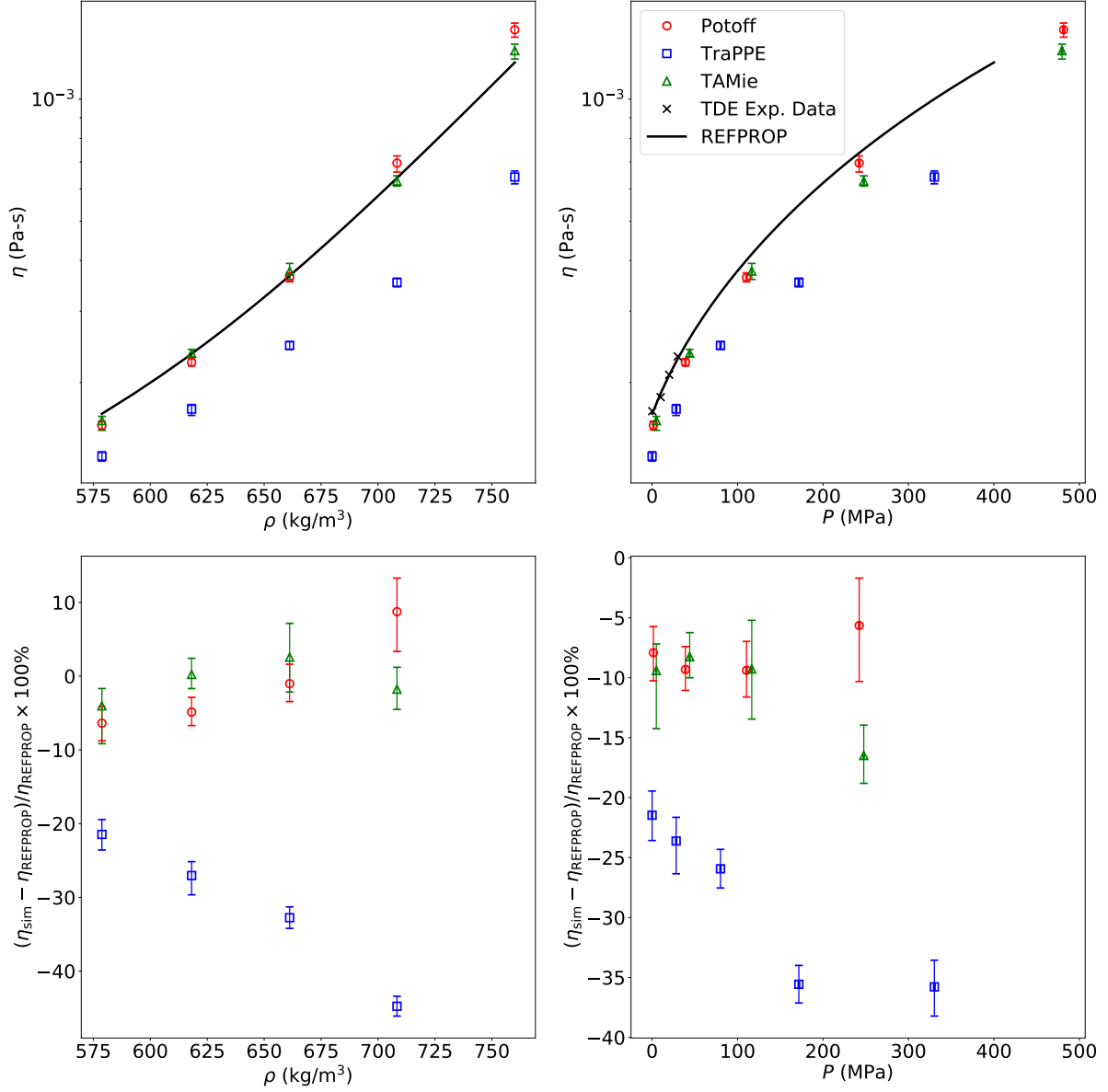    (a) Largest viscosity simulations are slow to converge and unclear if simulations are sufficiently long

Figure 7: Compressed liquid viscosities at 293 K for $n$-butane. Colors/symbols denote different force fields.

    (b) Tail-corrections could impact dynamics

    (c) Using REFPROP saturation conditions instead of force fields

## 4.1. $\rho_{\text{liq}}^{\text{sat}}$

There are at least three reasons why we perform simulations at the REFPROP $\rho_{\text{liq}}^{\text{sat}}$ instead of the force field $\rho_{\text{liq}}^{\text{sat}}$. First, this approach allows for a fair comparison of the force
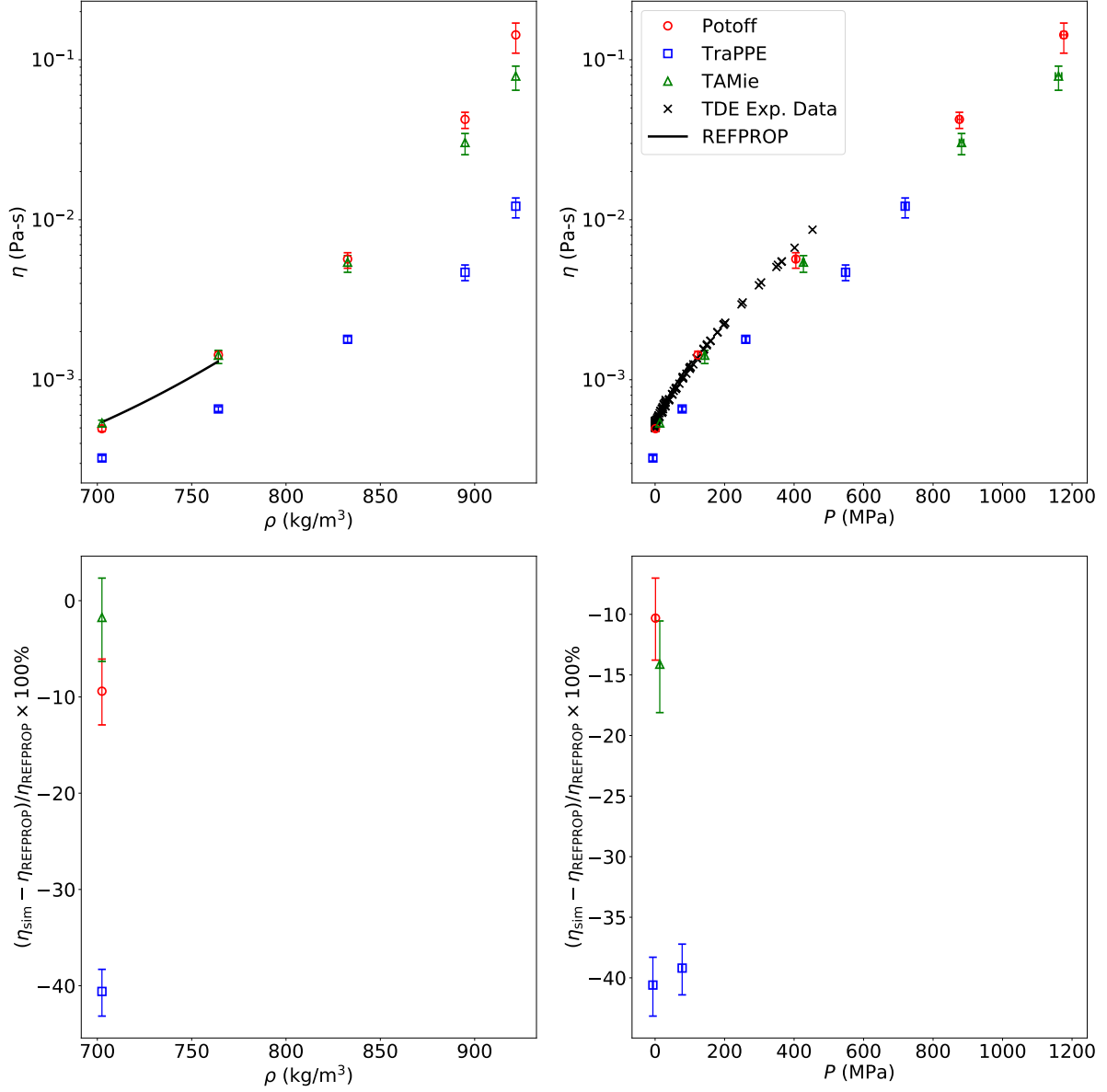
Figure 8: Compressed liquid viscosities at 293 K for *n*-octane. Colors/symbols denote different force fields.

fields' ability to predict viscosity, without penalizing force fields which are less accurate at predicting $\rho_{\text{liq}}^{\text{sat}}$ or rewarding force fields that mask their deficiencies in predicting viscosity by over- or under-estimating $\rho_{\text{liq}}^{\text{sat}}$. Second, since each of the studied force fields utilized $\rho_{\text{liq}}^{\text{sat}}$ data in their optimization, deviations between the REFPROP and force field values are small, typically less than 1 %. However, small differences in density have been reported to result
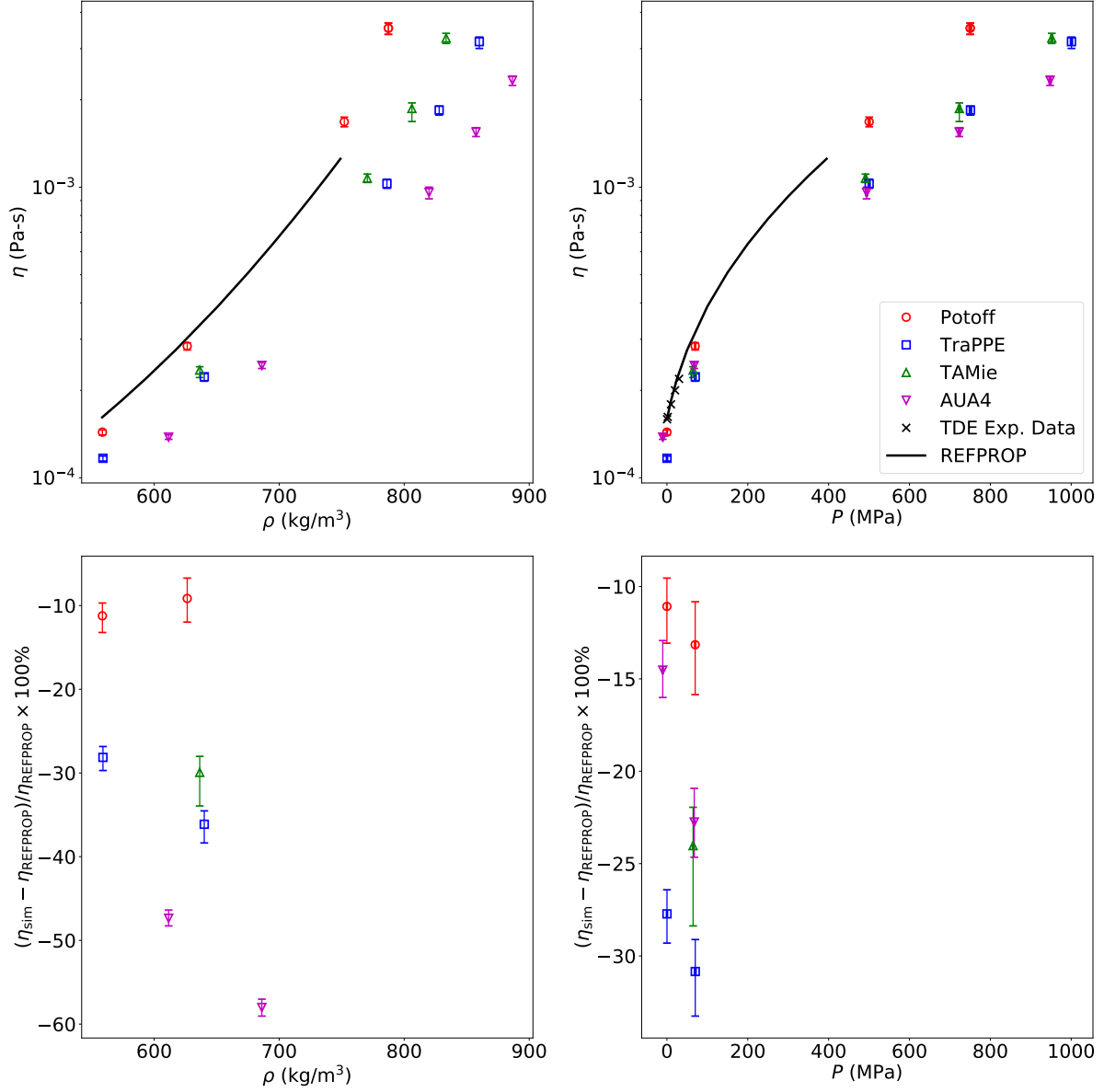
Figure 9: Compressed liquid viscosities at 293 K for 2-methylpropane. Colors/symbols denote different force fields.

in large differences in viscosity. For this reason, a small set of validation simulations are performed to determine the variability caused by utilizing the REFPROP densities. The force field saturated liquid densities were obtained from the literature.

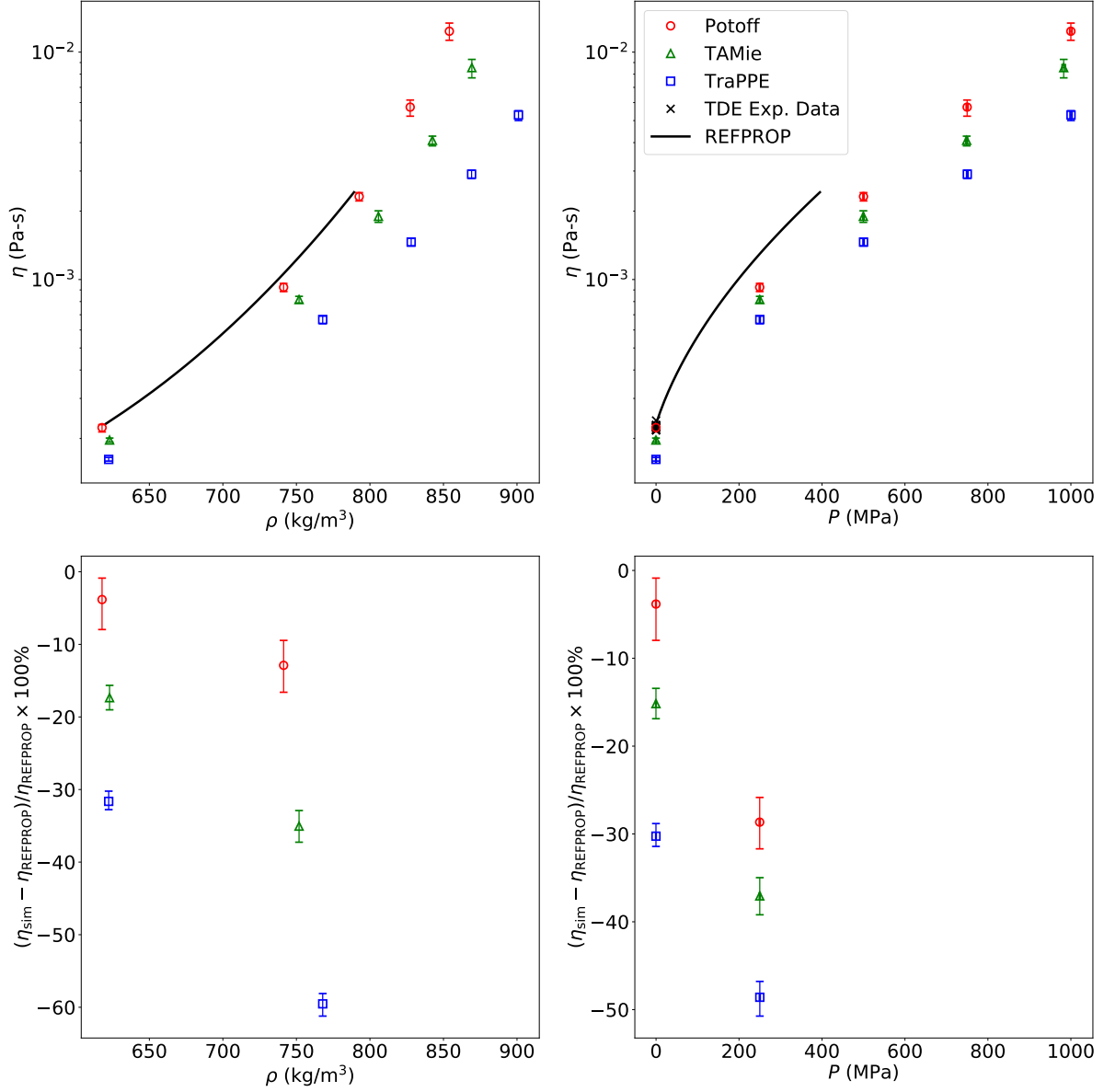The use of REFPROP $\rho_{\mathrm{liq}}^{\mathrm{sat}}$ caused some simulations to be in a meta-stable state. Specif-

Figure 10: Compressed liquid viscosities at 293 K for 2-methylbutane. Colors/symbols denote different force fields.

ically, this occurs when the force field vapor pressure is less than the REFPROP vapor pressure. Fortunately, this is uncommon as Potoff, TAMie, and AUA4 are quite reliable for estimating $P_{\text{vap}}^{\text{sat}}$ and TraPPE significantly over-estimates $P_{\text{vap}}^{\text{sat}}$.
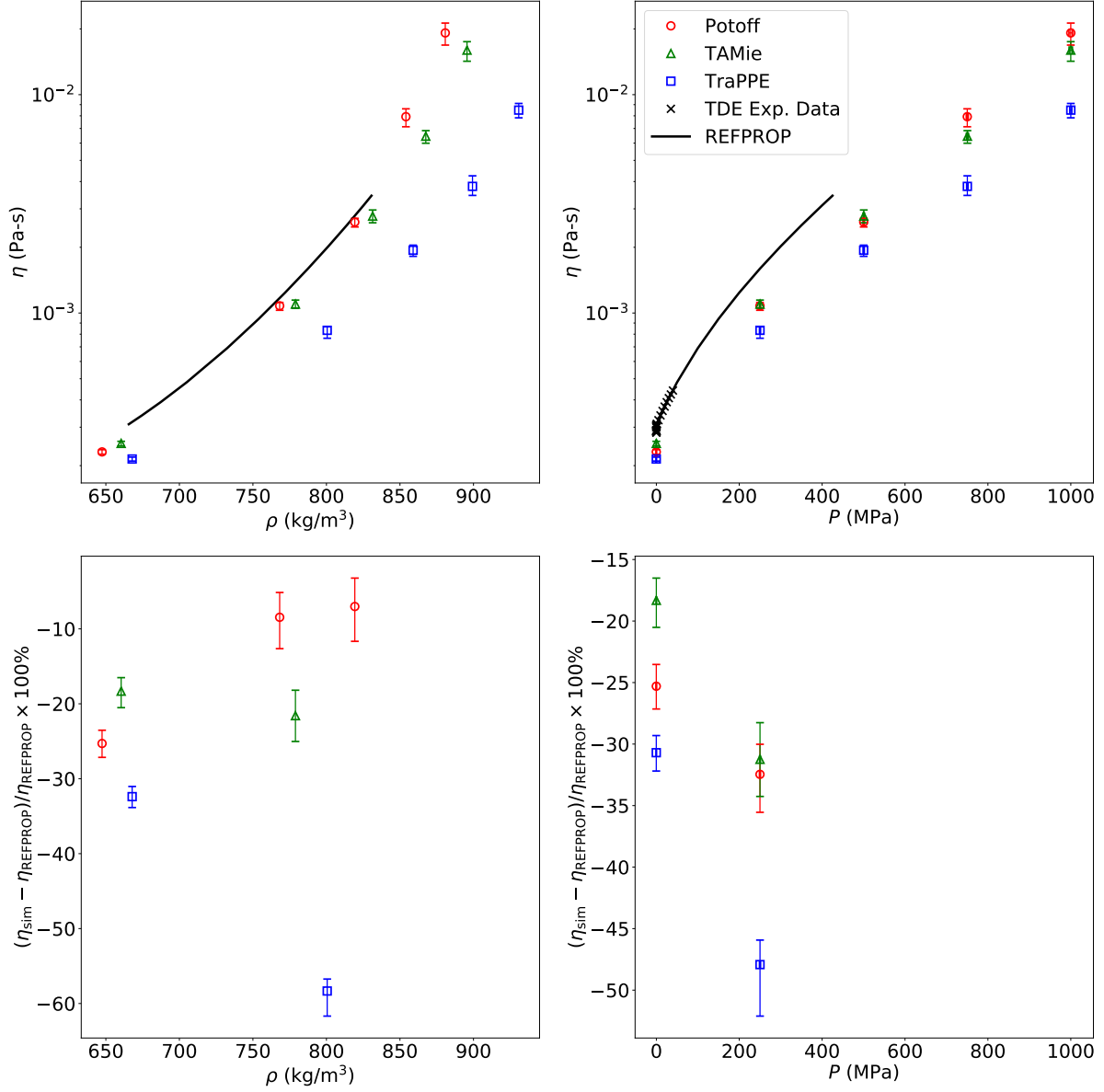
Figure 11: Compressed liquid viscosities at 293 K for 3-methylpentane. Colors/symbols denote different force fields.

## 5. Conclusions

This study demonstrates the improvement that has taken place over the past two decades for predicting viscosity with molecular simulation. First, the "Best Practices" for EMD lead to more reproducible results. Second, the state-of-the-art Mie n-6 force fields are significantly
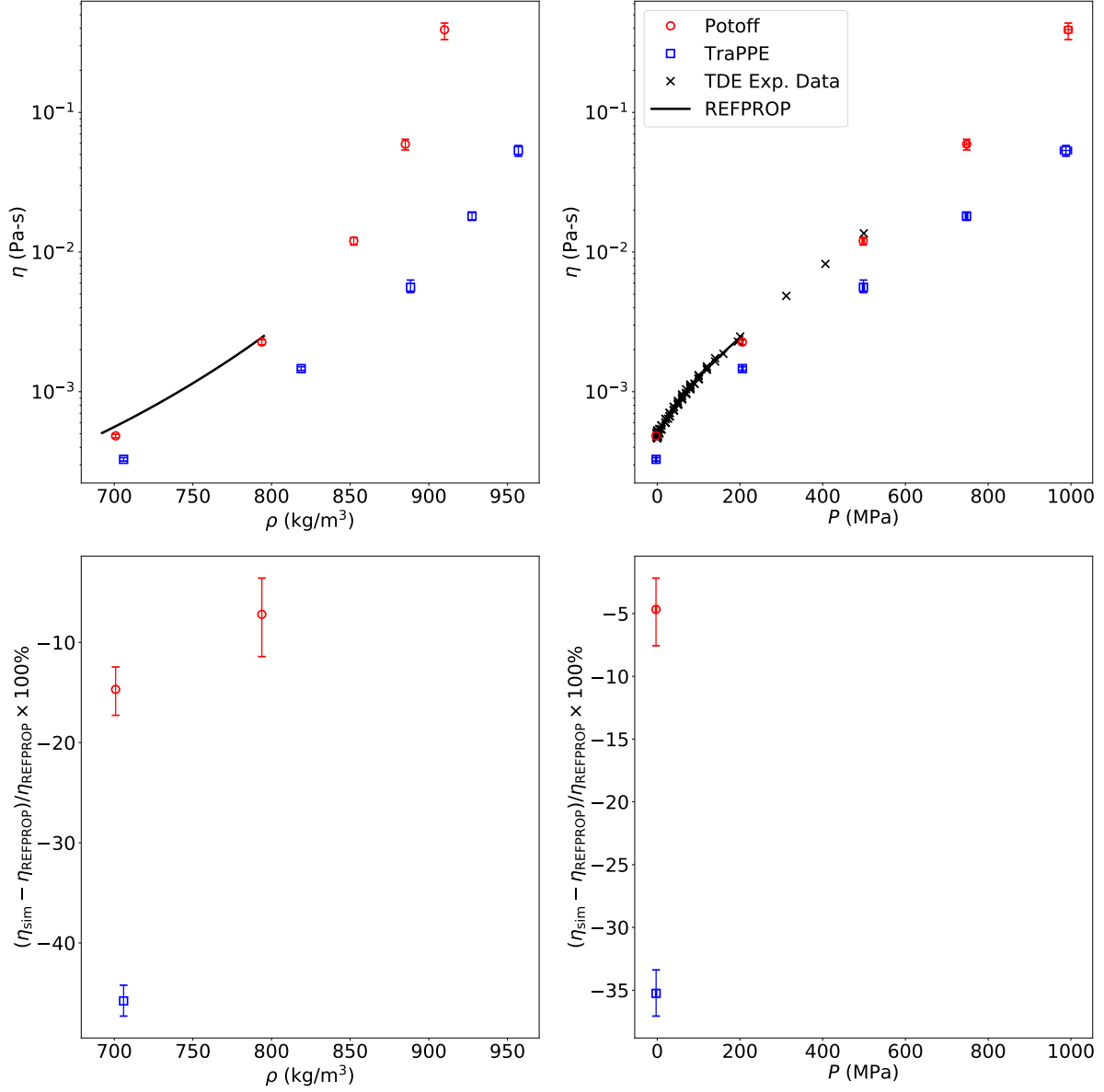
Figure 12: Compressed liquid viscosities at 293 K for 2,2,4-trimethylpentane. Colors/symbols denote different force fields.

more accurate than the traditional Lennard-Jones 12-6 force fields. More specifically, the Potoff and TAMie force fields typically predict saturated liquid viscosities for $n$-alkanes to within 10 % of the REFPROP values. By contrast, the TraPPE and AUA4 models under-predict saturated liquid viscosities by 30 % to 50 %, where the deviations are largest at

lower temperatures. While Potoff and TAMie are also more reliable for branched alkanes, deviations are larger and demonstrate a similar temperature dependence. The key limitation of the Potoff force field is that the choice of n= 16 is too repulsive at high densities, which causes the viscosity to be over-estimated at high densities. Due to a fortuitous cancellation of errors, the Potoff potential does provide a reliable $\eta$-$P$ trend. Since TAMie uses n= 14, the $\eta$-$\rho$ trend is slightly more reliable than that of Potoff.

## Acknowledgments

## References

[1] Carmelo Herdes, Tim S. Totton, and Erich A. Müller. Coarse grained force field for the molecular simulation of natural gases and condensates. *Fluid Phase Equilibria*, 406:91 − 100, 2015.

[2] M. G. Martin and J. I. Siepmann. Transferable potentials for phase equilibria. 1. United-atom description of n-alkanes. *The Journal of Physical Chemistry B*, 102(14):2569–2577, 1998.

[3] Marcus G. Martin and J. Ilja Siepmann. Novel configurational-bias monte carlo method for branched molecules. Transferable Potentials for Phase Equilibria. 2. United-Atom Description of Branched Alkanes. *The Journal of Physical Chemistry B*, 103(21):4508– 4517, 1999.

[4] Mansi S. Shah, J. Ilja Siepmann, and Michael Tsapatsis. Transferable potentials for

phase equilibria. Improved united-atom description of ethane and ethylene. *AIChE Journal*, 63(11):5098–5110, 2017.

[5] J. J. Potoff and D. A. Bernard-Brunel. Mie potentials for phase equilibria calculations: Applications to alkanes and perfluoroalkanes. *The Journal of Physical Chemistry B*, 113(44):14725–14731, 2009.

[6] Jason R. Mick, Mohammad Soroush Barhaghi, Brock Jackman, Loren Schwiebert, and Jeffrey J. Potoff. Optimized mie potentials for phase equilibria: Application to branched alkanes. *Journal of Chemical & Engineering Data*, 62(6):1806–1818, 2017.

[7] Philippe Ungerer, Christele Beauvais, Jerome Delhommelle, Anne Boutin, Bernard Rousseau, and Alain H. Fuchs. Optimization of the anisotropic united atoms inter-molecular potential for n-alkanes. *The Journal of Chemical Physics*, 112(12):5499–5510, 2000.

[8] Carlos Nieto-Draghi, Anthony Bocahut, Benoît Creton, Pascal Have, Aziz Ghoufi, Au-rélie Wender, , Anne Boutin, Bernard Rousseau, and Laurent Normand. Optimisation of the dynamical behaviour of the anisotropic united atom model of branched alka-nes: application to the molecular simulation of fuel gasoline. *Molecular Simulation*, 34(2):211–230, 2008.

[9] Andrea Hemmen and Joachim Gross. Transferable anisotropic united-atom force field based on the Mie potential for phase equilibrium calculations: n-alkanes and n-olefins. *The Journal of Physical Chemistry B*, 119(35):11695–11707, 2015.

[10] Dominik Weidler and Joachim Gross. Transferable anisotropic united-atom force field based on the mie potential for phase equilibria: Aldehydes, ketones, and small cyclic alkanes. *Industrial & Engineering Chemistry Research*, 55(46):12123–12132, 2016.

[11] M. P. Allen and D. J. Tildesley. *Computer Simulation of Liquids*. Clarendon Press ; Oxford University Press, Oxford England New York, 1987.

[12] M.J. Abraham, D. van der Spoel, E. Lindahl, B.Hess, and the GROMACS development team. *GROMACS User Manual version 2018, www.gromacs.org (2018)*, 2018.

[13] GROMACS non-bonded tail corrections assume that the long-range contribution from the $r^{-\lambda}$ term is negligible compared to the $r^{-6}$ term. By comparing the GROMACS output with other (slower) simulation packages, we verified that the small error introduced with this approximation does not significantly affect our results. For this reason, although it is straightforward to include the $r^{-\lambda}$ contribution, we did not attempt to modify the GROMACS default tail correction values.

[14] E. W. Lemmon, M. L. Huber, and M. O. McLinden. NIST Standard Reference Database 23: Reference Fluid Thermodynamic and Transport Properties-REFPROP, Version 9.1, National Institute of Standards and Technology, 2013.

[15] D. Bücker and W. Wagner. A reference equation of state for the thermodynamic properties of ethane for temperatures from the melting line to 675 K and pressures up to 900 MPa. *Journal of Physical and Chemical Reference Data*, 35(1):205–266, 2006.

[16] Eric W. Lemmon, Mark O. McLinden, and Wolfgang Wagner. Thermodynamic properties of propane. iii. a reference equation of state for temperatures from the melting line to 650 K and pressures up to 1000 MPa. *Journal of Chemical & Engineering Data*, 54(12):3141–3180, 2009.

[17] D. Bücker and W. Wagner. Reference equations of state for the thermodynamic properties of fluid phase n-butane and isobutane. *Journal of Physical and Chemical Reference Data*, 35(2):929–1019, 2006.

[18] R. Beckmueller, M. Thol, and R. Span. Fundamental equation of state for n-octane. *International Journal of Thermophysics*, Pending publication, 2018.

[19] Eric W. Lemmon and Roland Span. Short fundamental equations of state for 20 industrial fluids. *Journal of Chemical & Engineering Data*, 51(3):785–850, 2006.

[20] T.M. Blackham, A.K. Lemmon, and E.W. Lemmon. Fundamental equation of state for isooctane. *International Journal of Thermophysics*, Pending publication, 2018.

## 6. Supporting Information

### 6.1. Gromacs input files

1. Include all the .gro files
2. Include all the .top file templates
3. Include .mdp files
4. Or we can just include an example and then refer them to the GitHub website

### 6.2. Tabulated values

1. Ethane
   (a) Saturation
      i. Potoff
      ii. TraPPE
      iii. AUA4
      iv. TAMie
   (b) T293 highP
      i. Potoff
      ii. TraPPE
      iii. AUA4
      iv. TAMie
2. Propane
   (a) Saturation
      i. Potoff
      ii. TraPPE
      iii. AUA4
      iv. TAMie

    (b) T293 highP

        i. Potoff

        ii. TraPPE

        iii. AUA4

        iv. TAMie

3. n-Butane

    (a) Saturation

        i. Potoff

        ii. TraPPE

        iii. AUA4

        iv. TAMie

    (b) T293 highP

        i. Potoff

        ii. TraPPE

        iii. AUA4

        iv. TAMie

Repeat for all other compounds with corresponding potentials

## 6.3. *Finite-size effects*

1. Simulation results for 100, 200, 400, and 800 molecules

## 6.4. *Simulation length effects*

1. Verified that 1 ns is long enough for larger compounds

## 6.5. *Validation Runs*

1. Ethane NIST

2. n-Octane Literature

## 6.6. *Bond types, Harmonic vs LINCS*

1. Propane and n-butane with harmonic (arbirary bond constant) shows systematic increase

*6.7. Green-Kubo analysis*

1. Raw data, i.e., multiple replicates with the average

2. Exclude low time data and have a heurestic for determining the cut-off time

Example analysis, i.e., bootstrap distribution, replicates

*6.8. MCMC?*